Collision-Induced Dissociation and Theoretical Studies of Mg^+ Complexes with CO, CO_2, NH_3, CH_4, CH_3OH, and C_6H_6

Amity Andersen,[†] Felician Muntean, Derek Walter,[†] Chad Rue, and P. B. Armentrout*

Department of Chemistry, University of Utah, Salt Lake City, Utah 84112

Received: August 25, 1999; In Final Form: November 5, 1999

The sequential bond energies for complexes of Mg^+ with CO, CO_2, NH_3, CH_4, CH_3OH, and C_6H_6 are determined by collision-induced dissociation (CID) with xenon or argon in a guided ion beam tandem mass spectrometer. The kinetic energy dependence of the CID and ligand exchange cross sections are analyzed to yield 0 and 298 K bond energies for Mg^+−L after accounting for the effects of multiple ion−molecule collisions, internal energy of the reactant ions, and dissociation lifetimes. Bond energies (in eV) to Mg^+ at 0 K are determined for L = Ar (0.10 ± 0.07), Xe (0.32 ± 0.12), 1−2 CO (0.43 ± 0.06 and 0.40 ± 0.03), 1−3 CO_2 (0.60 ± 0.06, 0.50 ± 0.03, and 0.46 ± 0.06), 1−5 NH_3 (1.60 ± 0.12, 1.27 ± 0.07, 0.99 ± 0.09, 0.45 ± 0.11, and 0.58 ± 0.12), 1−2 CH_4 (0.29 ± 0.07 and 0.15 ± 0.07), 1−3 CH_3OH (1.51 ± 0.07, 1.25 ± 0.07, and 0.95 ± 0.09), and one C_6H_6 (1.39 ± 0.10 eV). As expected for largely electrostatic interactions, the sequential bond energies generally decrease monotonically with increasing number of ligands. These values are in good agreement with theoretical values in the literature and ab initio calculations performed here, but the agreement is mixed for comparison with results of photodissociation measurements. Qualitatively, geometries of these complexes are controlled by interactions of the ligands with the single polarized valence electron on Mg^+.

Introduction

Complexes of Mg^+ with small molecules have been studied by several groups. The earliest studies were performed by Operti et al. using Fourier transform ion cyclotron resonance mass spectrometry (FTICR).[1,2] Equilibrium studies for ligand exchange reactions of several oxygen-containing organic molecules were used to measure relative Mg^+ bond dissociation energies (BDEs). These were placed on an absolute scale by low-resolution threshold photodissociation measurements of $Mg^+(CH_3OH)$ among other complexes and later of $Mg^+(H_2O)$. Using a pulsed supersonic nozzle source, Duncan and co-workers have formed complexes of Mg^+ with the rare gases (Ar, Kr, and Xe),[3] H_2O, D_2O,[4] CO_2,[5] and benzene[6] and interrogated these complexes using high-resolution photodissociation spectroscopy. A Birge−Sponer extrapolation of the vibrational progression is used to extract BDEs of the first six complexes. In the $Mg^+(C_6H_6)$ system, threshold measurements of the dissociation energy were obtained by scanning the frequency of the photodissociation laser. Our laboratory has used threshold collision-induced dissociation methods to measure the BDEs of the $Mg^+(H_2O)_x$, where $x = 1-4$ complexes,[7] and compared these with similar hydrated clusters of Na^+ and Al^+. Hydrated magnesium ions have also been studied by Fuke and co-workers[8,9] and Castleman and co-workers,[10] and an interesting dehydrogenation reaction that depends on the number of waters is observed. Such a reaction is also observed in studies of $Mg^+(CH_3OH)_x$ complexes.[10−13] Photodissociation spectroscopy of $Mg^+(CH_4)$ has also been conducted by Kleiber and co-workers.[14]

Augmenting these experimental studies has been the extensive theoretical work of Bauschlicher and co-workers.[15−24] Calculations on $Mg^+(H_2O)_x$ and $Mg^+(CH_3OH)_x$ complexes have also been carried out by others.[10,12,25] Except in the cases of Mg^+-(Ar) and $Mg^+(CO_2)$, the theoretical BDEs differ quite dramatically with the photodissociation values. Reasonable agreement between theory and our CID BDEs for $Mg^+(H_2O)_x$ ($x = 1-4$) was obtained. One of the most interesting findings of the theoretical results is that the geometries of the $Mg^+(L)_x$ complexes are strongly influenced by interactions between the ligands and the valence electron, which is found to polarize significantly away from the ligands. Hence, the structures of $Mg^+(L)_2$ are bent in contrast to $Na^+(L)_2$ complexes that show linear L−M−L geometries, and larger complexes are similarly distorted.

In the present work, we examine the collision-induced dissociation (CID) of Mg^+ complexes with up to two CO, three CO_2, five NH_3, two CH_4, three CH_3OH, and one C_6H_6 molecules. This complements our previous studies of the CID of Mg^+ complexes with one to four water molecules.[7] Analysis of the kinetic energy dependent cross sections allows us to extract sequential bond dissociation energies for these species along with those for $MgAr^+$ and $MgXe^+$, species formed in ligand-exchange reactions. These results can then be compared with the extensive literature thermochemistry available for most of these Mg^+ complexes. The trends in the sequential bond energies are examined and variations in this thermochemistry from ligand to ligand are discussed.

Our detailed analysis of CID data requires vibrational frequencies and rotational constants for metal ligand complexes. Therefore, we performed theoretical calculations at the MP2-(full)/6-31G* level on all complexes considered experimentally along with those for $Mg^+(H_2O)_x$ considered previously.[7] These

* Corresponding author. E-mail: armentrout@chemistry.utah.edu.
[†] Present address: Department of Chemistry and Biochemistry, UCLA, Los Angeles, CA 90095.

10.1021/jp993031t CCC: $19.00
Published on Web 01/06/2000

calculations also provide geometrical structures that help us visualize the complexes, which allows a better understanding of the trends in the thermochemistry obtained. In addition, we calculate BDEs at 0 K using single-point calculations at the MP2(full)/6-311+G(2d,2p) level including zero-point and basis set superposition error corrections. This provides a systematic comparison with the present experimental bond dissociation energies.

Experimental and Computational Section

General Experimental Procedures. Cross sections for the collision-induced dissociation (CID) of Mg^+−ligand complexes are measured using a guided ion beam tandem mass spectrometer. A complete description of the apparatus and experimental procedures is provided elsewhere.[26,27] Mg^+ complex ions produced by a dc-discharge/flow tube source[28] are extracted from the source, accelerated, and focused into a magnetic sector momentum analyzer for mass analysis. Mass-selected ions are decelerated to a desired kinetic energy and focused into an octopole ion guide that traps the ions in the radial direction and ensures efficient collection of reactant and product ions. The octopole passes through a static gas cell containing xenon or argon. Pressure of the collision gas (Xe or Ar) in the gas cell is kept relatively low (0.05−0.20 mTorr) to avoid multiple collisions. Product and reactant ions drift to the end of the octopole where they are directed into a quadrupole mass filter for mass analysis and then detected by a secondary electron-scintillator-phototube detector. Ion intensities are converted to absolute cross sections as described previously.[26] Absolute uncertainties in cross sections, which are largely a result of uncertainties in the pressure measurement and the length of the interaction region, are about ±20%. Ion kinetic energies in the laboratory frame, E_{lab}, are converted to energies in the center-of-mass frame, E_{CM}, using the formula $E_{CM} = E_{lab}m/(m + M)$, where M and m are the masses of the reactant ion and neutral, respectively. The absolute zero and distribution of the ion kinetic energies are determined using the octopole ion guide as a retarding potential analyzer as previously described.[26] Because the reaction zone and energy analysis region are physically the same, ambiguities in the energy analysis resulting from contact potentials, space charge effects, and focusing aberrations are minimized.[26] The absolute uncertainty in the energy scale is ±0.05 eV (lab). The ion kinetic energy distributions are nearly Gaussian with a fwhm of 0.2−0.4 eV (lab).

Ion Source. Magnesium ion−ligand clusters are formed in a 1 m long flow tube operating at a pressure of 500−700 mTorr with a helium flow rate of 4000−7000 sccm. Atomic Mg^+ ions are generated by a continuous dc discharge source. This source consists of a water-cooled metal rod maintained at high negative voltage, typically 1−3 kV. A cap of magnesium metal covers the end of the metal rod and acts as the cathode. A mixture of a 5−7% argon in helium flows over the cathode and is ionized by the dc field. Neutral and ionic metal atoms are sputtered off the cathode by accelerated argon ions and swept out with the flow. Neutral gases are introduced about 50 cm downstream in the flow tube to form metal complexes by three-body association. Complex ions undergo about 10^5 collisions with the carrier gases before they exit the flow tube. It is assumed that the complexes produced are in their electronic ground states and that the internal energy of these complexes is well-described by a Boltzmann distribution at room temperature. Previous work from this laboratory has shown that these assumptions are usually valid.[28−32]

Data Analysis. Threshold regions of the reaction cross sections are modeled using eq 1 where σ_0 is an energy-independent scaling factor, E is the relative translational energy of the reactants, E_0 is the threshold for the reaction at 0 K, and n is an adjustable parameter. The summation is over the rovibrational states of the reactant ions. E_i is the excitation energy of each state and g_i is the population of those states ($\sum g_i = 1$). The Beyer−Swinehart algorithm[33] is used to calculate the distribution of vibrational energy at 298 K from the vibrational frequencies for each complex. Frequencies of normal vibrational modes for each complex were calculated using ab initio methods described below. The effect of the uncertainty in the frequencies on the threshold determination was estimated by scaling the frequencies up and down by 10%.

$$\sigma(E) = \sigma_0 \sum g_i (E + E_i - E_0)^n / E \qquad (1)$$

We also consider the possibility that collisionally activated complex ions do not dissociate on the time scale of our experiment (about 10^{-4} s) by including statistical theories for unimolecular dissociation into eq 1 as described in detail elsewhere.[30,34] This requires sets of rovibrational frequencies appropriate for the energized molecules and the transition states (TSs) leading to dissociation. As in other recent studies of CID processes, the largely electrostatic interaction binding the complexes means that the dissociation TSs are loose and occur at the centrifugal barrier for interaction of $Mg^+(L_{x-1})$ with the neutral ligand. The TS is located variationally and the molecular parameters are treated in a phase space limit (PSL), as described in detail elsewhere.[35] We treat the 2-D external rotations of the complex adiabatically but with centrifugal effects included, consistent with the discussion of Waage and Rabinovitch.[36] In the present work, the adiabatic 2-D rotational energy is treated using a statistical distribution with the average rotational energy, as described in detail elsewhere.[35]

The model represented by eq 1 is expected to be appropriate for translationally driven reactions[37] and has been found to reproduce reaction cross sections well in a number of previous studies of both atom−diatom and polyatomic reactions,[38,39] including CID processes.[28,30,32,35,40−42] The model is convoluted with the kinetic energy distributions of both reactants,[26] and a nonlinear least-squares analysis of the data is performed to give optimized values for the parameters σ_0, E_0, and n. The error (reported as 1 standard deviation) associated with the measurement of E_0 is estimated from the range of threshold values determined for different data sets, variations associated with uncertainties in the vibrational frequencies, and the error in the absolute energy scale. For analyses that include the RRKM lifetime effect, uncertainties in the reported E_0 values also include the effects of increasing and decreasing the average time assumed available for dissociation (10^{-4} s) by a factor of 2.

Equation 1 explicitly includes the internal energy of the ion, E_i. All energy available is treated statistically, which should be a reasonable assumption because the internal (rotational and vibrational) energy of the reactants is redistributed throughout the ion upon impact with the collision gas. The threshold for dissociation is by definition the minimum energy required for dissociation and thus corresponds to formation of products with no internal excitation. The assumption that products formed at threshold have an internal temperature of 0 K has been tested for several systems.[28,30,32,34,35,42] It has been shown that treating all energy of the ion (vibrational, rotational, and translational) as capable of coupling into the dissociation coordinate leads to reasonable thermochemistry. The threshold energies for dissociation reactions determined by analysis with eq 1 are

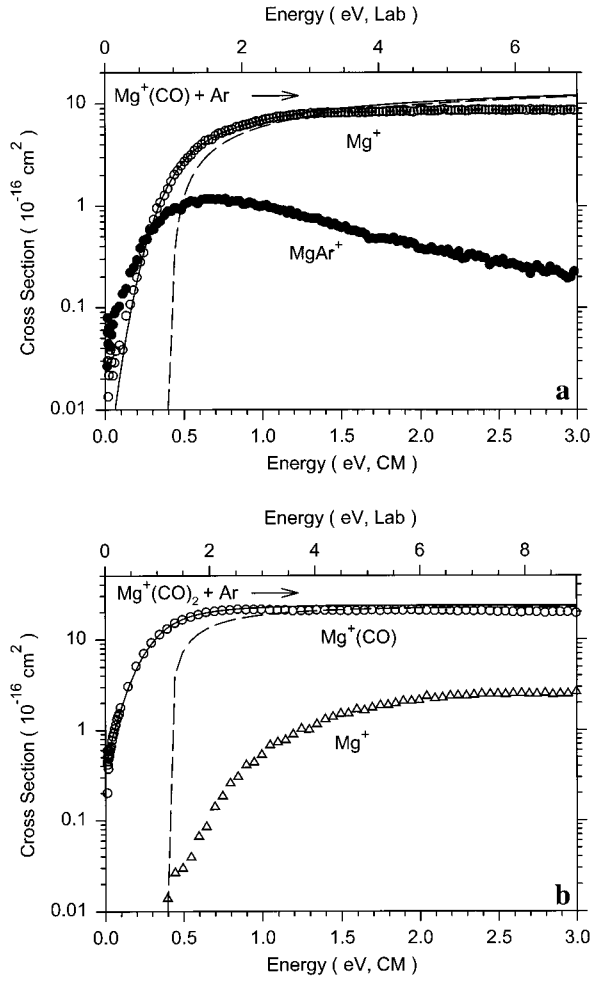

Figure 1. Cross sections for collision-induced dissociation of $Mg^+(CO)_x$ ($x = 1$ and 2) complexes with Ar as a function of kinetic energy in the center-of-mass frame (lower *x*-axis) and the laboratory frame (upper *x*-axis). Solid lines show the best fits to the CID cross sections using the model of eq 1 convoluted over the neutral and ion kinetic and internal energy distributions. Dotted lines show the model cross sections in the absence of experimental kinetic energy broadening for reactants with an internal energy of 0 K.

TABLE 1: Optimized Parameters of Eq 1 for CID of $Mg^+(CO)_x$ and $Mg^+(CH_4)_x$ Complexes with Ar[a]

reactant ion	product ion	σ_0	n	E_0, eV
$Mg^+(CO)$	Mg^+	11 (1)	1.1 (0.3)	0.43 (0.06)
	$MgAr^+$	1.5 (1)	0.8 (0.6)	0.31 (0.10)
$Mg^+(CO)_2$	$Mg^+(CO)$	33 (1)	0.9 (0.1)	0.40 (0.03)
	Mg^+	0.4 (0.1)	2.4 (0.2)	1.2 (0.2)
$Mg^+(CH_4)$	Mg^+	13 (1)	1.2 (0.4)	0.29 (0.07)
	$MgAr^+$	3 (1)	0.7 (0.2)	0.22 (0.04)
$Mg^+(CH_4)_2$	$Mg^+(CH_4)$	9 (1)	1.5 (0.1)	0.15 (0.07)
	Mg^+	0.5 (0.1)	1.8 (0.1)	0.49 (0.07)

[a] Uncertainties in parentheses.

converted to 0 K bond energies by assuming that E_0 represents the energy difference between reactants and products at 0 K.[43] This requires that there are no activation barriers in excess of the endothermicity of dissociation. This is generally true for ion−molecule reactions[38] and should be valid for the simple heterolytic bond fission reactions examined here.[44]

Computational Details. To obtain model structures, vibrational frequencies, and energetics for the neutral and metalated ligands, ab initio calculations were carried out using Gaussian 98W.[45] These calculations include all complexes studied here (except $MgXe^+$) and those for one to four H_2O ligands as well. Geometry optimizations were performed at the MP2(full)/6-31G* level.[46−48] This level of theory was recently determined by Hoyau et al.[49] and confirmed by us[50] to provide a good description of sodium cation complexes, so we presume it is adequate for the present systems as well. Vibrational analyses of the geometry-optimized structures were performed to determine the vibrational frequencies and rotational constants of the molecules and to confirm that the geometries located correspond to stable minima on the global potential energy surface. Such constants are listed in Tables S1 and S2, available in the Supporting Information. When used to model the data or to calculate thermal energy corrections, the MP2(full)/6-31G* vibrational frequencies are scaled by a factor of 0.9646, as documented elsewhere.[51]

Single point energy calculations were performed at the MP2(full)/6-311+G(2d,2p) level using the MP2(full)/6-31G* geometries. To obtain accurate 0 K bond dissociation energies, the computed equilibrium bond energies, D_e, were corrected for zero-point energies (ZPEs) and basis set superposition errors (BSSE) were subtracted in the full counterpoise approximation.[52,53] Such BSSE corrections have proven valuable in getting good agreement with experiment in several studies of Na^+−ligand bond energies.[49,50,54,55] The BSSE corrections ranged from 0.02 eV for $Mg^+(Ar)$ to 0.10 eV for the $Mg^+(C_6H_6)$ and $Mg^+(CH_3OH)_3$ complexes. Energies at both the MP2(full)/6-31G* and MP2(full)/6-311+G(2d,2p) levels of theory along with the ZPE and BSSE corrections are included in Table S3 in the Supporting Information. We also note that in the difficult case of CO,[16] we verified that the Mg^+−CO geometry was more stable than Mg^+−OC (by 0.29 eV) at this level of theory.

Experimental Results

Collision-induced dissociation (CID) of magnesium ion complexes, reaction 2, was examined over energy ranges

$$Mg^+(L_x) + Rg \rightarrow Mg^+(L_{x-1}) + L + Rg \qquad (2)$$

adequate to accurately determine the threshold for dissociation. In all cases, the dependence of the CID cross sections on the pressure of the Rg collision partner was examined and cross sections were extrapolated to zero pressure[40] when such a dependence was observed. For most systems, Xe was used as the collision gas because translational to vibrational energy transfer is particularly efficient for this polarizable atom.[27,56,57] In the cases of the weakly bound $Mg^+(CO)_x$, $Mg^+(CO_2)_x$, and $Mg^+(CH_4)_x$ complexes, however, Ar was used as the collision gas for two reasons. Because Ar is less massive, the threshold region is spread over a wider range of laboratory energies which allows more precise variation of kinetic energy in the center-of-mass frame. In addition, for these weakly bound complexes, the ligand exchange process 3

$$Mg^+(L_x) + Rg \rightarrow Mg^+(L_{x-1})Rg + L \qquad (3)$$

can reach appreciable cross sections when Rg is Xe because the reaction can become exothermic. Competition between reactions 2 and 3 can influence the shape of the cross section for reaction 2, making its threshold analysis more difficult. Because Ar is much less polarizable than Xe, its binding energy is much lower and reaction 3 is suppressed. This is illustrated below.

CID of $Mg^+(CO)_x$. Results for the interaction of $Mg^+(CO)_x$ ($x = 1-2$) with Ar are shown in Figure 1. For $x = 1$, reactions 2 and 3 are both observed and have low threshold energies.

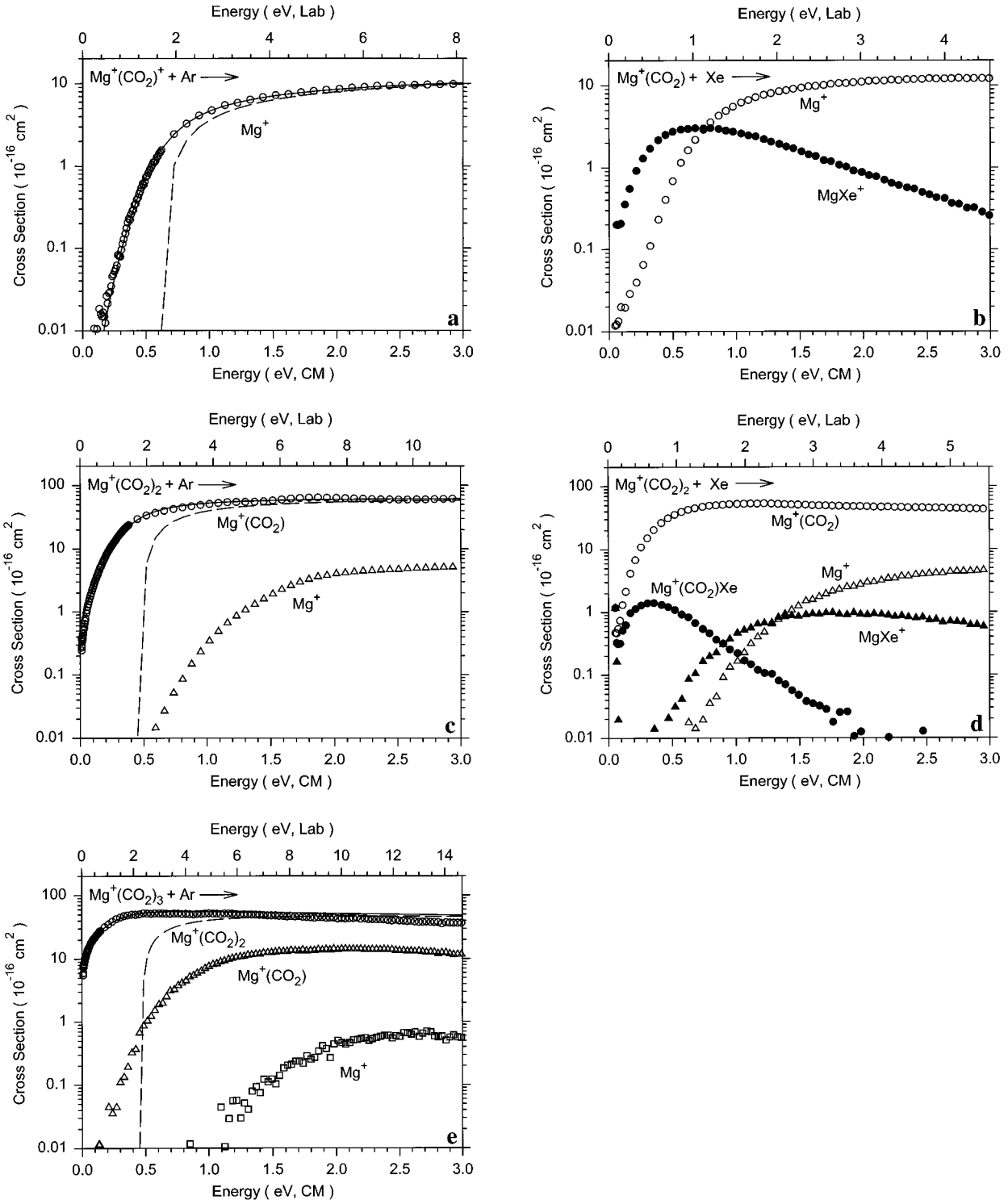

Figure 2. Cross sections for collision-induced dissociation of $Mg^+(CO_2)_x$ ($x = 1$ - 3) complexes with Ar and Xe as a function of kinetic energy in the center-of-mass frame (lower *x*-axis) and the laboratory frame (upper *x*-axis). Solid lines show the best fits to the CID cross sections using the model of eq 1 convoluted over the neutral and ion kinetic and internal energy distributions. Dotted lines show the model cross sections in the absence of experimental kinetic energy broadening for reactants with an internal energy of 0 K.

The ligand-exchange reaction 3 has a slightly lower threshold than the CID process 2 but is clearly endothermic, indicating that $D(Mg^+-Ar) < D(Mg^+-CO)$. As the energy is increased, the $MgAr^+$ cross section declines, indicating that this product undergoes dissociation to yield Mg^+. For $x = 2$, only sequential ligand losses are observed. Ligand exchange processes probably occur but have cross sections too small to be easily observed. The quantitative analysis of these cross sections using eq 1 is reported in Table 1. It can be seen in Figure 1 that the reproduction of the data is very good over extended ranges of both energy and cross section magnitude. The measured E_0 values confirm that the threshold for loss of a single ligand from $x = 2$ is only slightly lower than that from $x = 1$. The main difference between the appearance of the two cross sections is attributable to the greater internal energy content of the $Mg^+(CO)_2$ complex.

CID of $Mg^+(CO_2)_x$. Results for the interaction of $Mg^+(CO_2)_x$ ($x = 1-3$) with Ar and Xe are shown in Figure 2. For $x = 1$

TABLE 2: Optimized Parameters of Eq 1 for CID of $Mg(CO_2)_x^+$ Complexes with Ar and Xe[a]

reactant system	product ion	σ_0	n	E_0, eV
$Mg^+(CO_2) + Ar$	Mg^+	12 (1)	1.2 (0.2)	0.60 (0.06)
$Mg^+(CO_2) + Xe$	Mg^+	14 (2)	1.1 (0.1)	0.63 (0.11)
	$MgXe^+$	3.7 (0.3)	0.6 (0.1)	0.33 (0.03)
$Mg^+(CO_2)_2 + Ar$	$Mg^+(CO_2)$	81 (2)	1.0 (0.1)	0.50 (0.03)
$Mg^+(CO_2)_2 + Xe$	$Mg^+(CO_2)$	69 (2)	0.7 (0.1)	0.46 (0.09)
	Mg^+	6.1 (0.8)	1.3 (0.1)	1.27 (0.12)
	$Mg^+(CO_2)Xe$	2.9 (0.3)	1.0 (0.1)	0.27 (0.09)
	$MgXe^+$	1.8 (0.3)	1.0 (0.3)	0.92 (0.11)
$Mg^+(CO_2)_3 + Ar$	$Mg^+(CO_2)_2$	65 (6)	0.8 (0.2)	0.46 (0.06)[b]
$Mg^+(CO_2)_3 + Xe$	$Mg^+(CO_2)_2$	79 (27)	0.3 (0.2)	0.44 (0.13)
	$Mg^+(CO_2)$	39 (2)	1.2 (0.4)	0.90 (0.13)
	Mg^+	6.5 (1.7)	1.1 (0.3)	2.09 (0.26)

[a] Uncertainties in parentheses. [b] Lifetime shift = 0.014 eV.

and 2, the ligand exchange reactions with Xe are significant although endothermic in both cases, indicating that Xe is more weakly bound to Mg^+ and $Mg^+(CO_2)$ than CO_2. Competition between these reactions and simple CID is obvious as the former cross sections decrease rapidly once the threshold for CID is surpassed. With Ar, the ligand exchange reaction is much less important such that cross sections for these reactions are lost in the noise ($\sim 10^{-17}$ cm^2). Despite this competition, the CID cross sections with Ar and Xe are very similar.

Thresholds for loss of a single ligand occur at low energies for all three complexes and decrease as x increases. The magnitude of the total cross sections at high energies increases as x increases, although not directly in proportion to the number of ligands. In the case of $x = 3$, the cross section for loss of a single ligand declines as the cross section for loss of a second ligand increases, indicative of sequential dissociation. Loss of three ligands also occurs at high energies.

Analysis of these cross sections using eq 1 is reported in Table 2. Again, the reproduction of the data over wide energy and magnitude ranges is achieved (Figure 2). This quantitative analysis confirms the qualitative observations noted above for both cross section magnitudes, σ_0 values, and threshold energies, E_0. In these systems, the threshold analysis of the Ar and Xe data yields very similar thermochemistry, although thresholds from the Ar systems are more precise in all cases. Therefore, these results are used later for the thermochemistry derived.

CID of $Mg^+(NH_3)_x$. Cross section data for the CID of $Mg^+(NH_3)_x$ ($x = 1-5$) with Xe are shown in Figure 3. No ligand exchange processes are observed, indicating that their cross sections are probably less than about 10^{-17} cm^2. Sequential ligand loss is observed in all cases, although loss of more than three (two) ligands is not monitored for $x = 4$ (5), largely because the intensities of these beams were relatively small. The thresholds for loss of a single ligand decrease as x increases but ammonia clearly binds to Mg^+ much more strongly than CO or CO_2. The total cross sections at high energies increase from $x = 1$ to 4 while the magnitude of the cross section for $Mg^+(NH_3)_5$ is somewhat less than that for $Mg^+(NH_3)_4$. For $x = 3-5$, the cross sections for loss of a single ligand decline as the cross section for secondary ligand loss increases, indicative of sequential loss of single ligands. Analyses of these cross sections using eq 1 are reported in Table 3 and confirm the qualitative observations noted above. Fits to the data are very good. In the cases of $x = 3-5$, the models shown reproduce the total cross sections (rather than the cross section for loss of a single ligand) at higher energies because the $Mg^+(NH_3)_{x-1}$ cross sections are influenced by subsequent decomposition while this effect is not included in the model cross sections. This is shown explicitly in Figure 3e.

CID of $Mg^+(CH_4)_x$. Results for the interaction of $Mg^+(CH_4)$ with Ar and Xe are shown in Figure 4. The ligand-exchange reaction 3 is prominent in the Xe system. The cross section for this reaction declines with increasing energy, indicating that it is exothermic, or equivalently that $D(Mg^+-Xe) > D(Mg^+-CH_4)$. In contrast, ligand exchange with Ar is endothermic, establishing that $D(Mg^+-CH_4) > D(Mg^+-Ar)$. As with the CO and CO_2 systems, the threshold for loss of the methane ligand is quite low. The shape of the Mg^+ cross section in the $Mg^+(CH_4) + Xe$ system is strongly influenced by competition with the ligand exchange process. Comparison of this cross section with that obtained in the Ar system clearly shows that the CID process is suppressed at low energies. This makes analysis of the cross section in the Xe system problematic. In contrast, the competition between these reactions in the Ar system is much less severe such that the Mg^+ cross section rises much more rapidly from threshold. Results of analyses on the CID cross sections with Ar are listed in Table 1 and shown in Figure 4a.

We also formed a complex having the correct mass for $Mg^+(CH_4)_2$ complex and which lost CH_4 molecules sequentially, as expected. However, the $Mg^+(CH_4)$ cross section has two components and these ions (with a mass specified by using the ^{24}Mg isotope) also decomposed to form a product at 26 amu with a magnitude slightly greater than formation of $^{24}Mg^+$. While it is possible that this product could be decomposition to $MgH_2^+ + C_2H_6$, we think it unlikely that efficient σ bond activation is induced by this metal ion. Rather, we think it likely that the beam is contaminated with a second complex (possibly an oxide) that we cannot identify with certainty. Nevertheless, analysis of the $^{24}Mg^+$ channel is straightforward and unambiguous and allows a check on our analysis of the low-energy portion of the $Mg^+(CH_4)$ product cross section. Because of the likely contamination, the results are not shown and the derived values rather speculative, but as the analysis is informative and agrees well with theory, it is included in Table 1.

CID of $Mg^+(CH_3OH)_x$. Results for the interaction of $Mg^+(CH_3OH)_x$ ($x = 1-3$) with Xe are shown in Figure 5. The dominant process in all three systems is loss of a single ligand. The threshold for this process decreases with increasing x. Loss of a second ligand at higher energies is observed for the $x = 2$ and 3 systems. Ligand exchange processes are observed for both $x = 1$ and 2 complexes and are inefficient in both cases. Analysis of these cross sections using eq 1 is reported in Table 4. Figure 5 shows that the data are reproduced over about 5 eV and at least 2 orders of magnitude. For $x = 3$, the model reproduces the total cross section past the peak in the $Mg^+(CH_3OH)_2$ cross section, because the model does not include secondary dissociation processes.

Collisional activation of the $Mg^+(CH_3OH)_x$ complexes also leads to unusual reactions in which the C−O bond is activated in the high-energy processes 4 and 5.

$$Mg^+(CH_3OH)_x + Xe \rightarrow MgOH^+(CH_3OH)_y + CH_3 + (x - y - 1)CH_3OH + Xe \quad (4)$$

$$\rightarrow CH_3^+ + MgOH + (x - 1)CH_3OH + Xe \quad (5)$$

(It seems possible that these minor channels are the result of contaminants in the reactant ion beam, but no other ionic

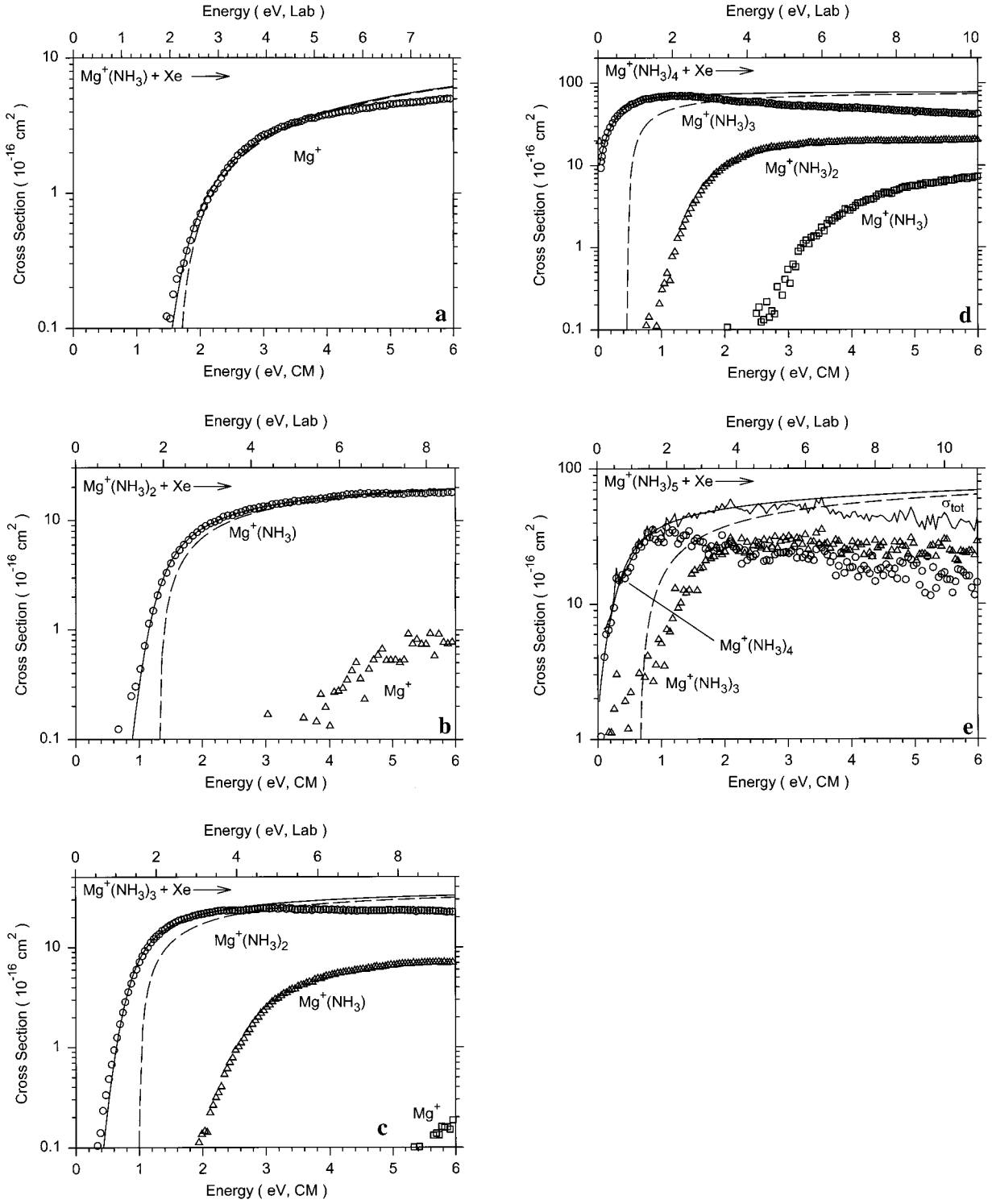

Figure 3. Cross sections for collision-induced dissociation of $Mg^+(NH_3)_x$ ($x = 1$ - 5) complexes with Xe as a function of kinetic energy in the center-of-mass frame (lower *x*-axis) and the laboratory frame (upper *x*-axis). Solid lines show the best fits to the CID cross sections using the model of eq 1 convoluted over the neutral and ion kinetic and internal energy distributions. Dotted lines show the model cross sections in the absence of experimental kinetic energy broadening for reactants with an internal energy of 0 K.

products that might identify such products as anything but the desired complexes were observed.) For process 4, all possible values of y (0 to $x - 1$) are observed, but oddly do not appear in the expected order, i.e., larger values of y should have lower thresholds and bigger cross sections. These reactions appear to be driven by formation of the stable $MgOH^+$ and CH_3^+ cations, which have closed-shell electronic configurations. Other possible processes, reactions 6, have been observed in other experiments for complexes with larger values of x.[11−13]

$$Mg^+(CH_3OH)_x + Xe \rightarrow MgOCH_3^+(CH_3OH)_y + H + (x - y - 1)CH_3OH + Xe \quad (6)$$

These reactions were not observed in the present studies; however, our sensitivity to these reactions is poor because these

TABLE 3: Optimized Parameters of Eq 1 for CID of $Mg^+(NH_3)_x$ Complexes with Xe[a]

reactant ion	product ion	σ_0	n	E_0, eV
$Mg^+(NH_3)$	Mg^+	5.5 (1.5)	1.4 (0.3)	1.60 (0.12)
$Mg^+(NH_3)_2$	$Mg^+(NH_3)$	20 (2)	1.1 (0.1)	1.27 (0.07)
	Mg^+	1.0 (0.3)	1.5 (0.2)	3.1 (0.1)
$Mg^+(NH_3)_3$	$Mg^+(NH_3)_2$	36 (2)	1.0 (0.1)	0.99 (0.09)
	$Mg^+(NH_3)$	7.4 (1.1)	1.7 (0.2)	2.2 (0.1)
	Mg^+	0.7 (0.4)	1.5 (0.6)	4.8 (0.4)
$Mg^+(NH_3)_4$	$Mg^+(NH_3)_3$	80 (2)	1.0 (0.1)	0.45 (0.11)[b]
	$Mg^+(NH_3)_2$	31 (2)	1.2 (0.1)	1.7 (0.1)
	$Mg^+(NH_3)$	14 (4)	1.1 (0.2)	3.5 (0.3)
$Mg^+(NH_3)_5$	$Mg^+(NH_3)_4$	52 (4)	1.2 (0.2)	0.58 (0.12)[c]
	$Mg^+(NH_3)_3$	20 (1)	2.2 (0.4)	0.9 (0.2)

[a] Uncertainties in parentheses. [b] Lifetime shift = 0.02 eV. [c] Lifetime shift = 0.06 eV.

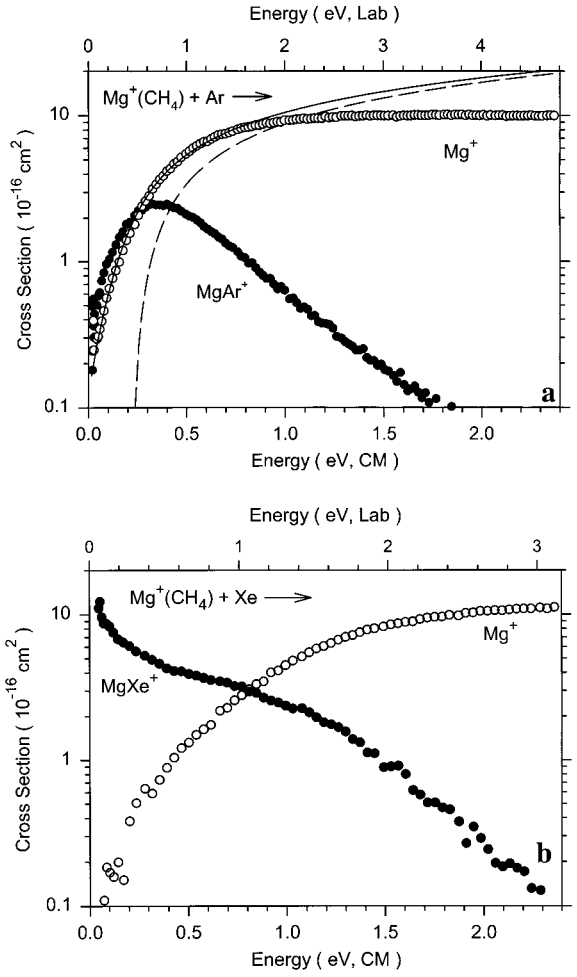

Figure 4. Cross sections for collision-induced dissociation of $Mg^+(CH_4)$ complexes with Ar and Xe as a function of kinetic energy in the center-of-mass frame (lower *x*-axis) and the laboratory frame (upper *x*-axis). The solid line shows the best fit to the CID cross section using the model of eq 1 convoluted over the neutral and ion kinetic and internal energy distributions. The dotted line shows the model cross section in the absence of experimental kinetic energy broadening for reactants with an internal energy of 0 K.

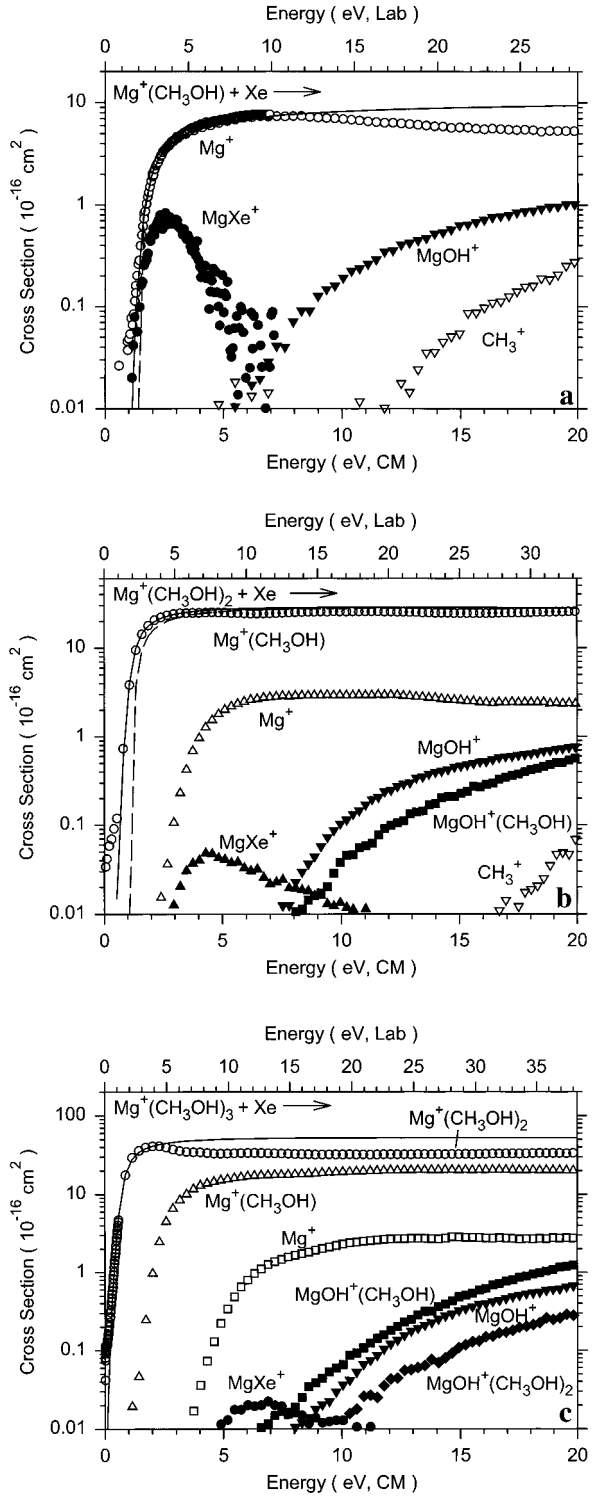

Figure 5. Cross sections for collision-induced dissociation of $Mg^+(CH_3OH)_x$ ($x = 1-3$) complexes with Xe as a function of kinetic energy in the center-of-mass frame (lower *x*-axis) and the laboratory frame (upper *x*-axis). Solid lines show the best fits to the CID cross sections using the model of eq 1 convoluted over the neutral and ion kinetic and internal energy distributions. Dotted lines show the model cross sections in the absence of experimental kinetic energy broadening for reactants with an internal energy of 0 K.

product ions lie only 1 amu below the mass of the very intense reactant ions.

To consider the thermochemistry of these reactions, we require the following data: $D_0(CH_3-OH) = 3.92 \pm 0.02$ eV,[58] $IE(CH_3) = 9.843 \pm 0.002$ eV,[58] $D_0(Mg^+-OH) = 3.25 \pm 0.17$ eV,[2] and $IE(MgOH) = 7.3 \pm 0.1$[2] or 7.5 ± 0.3 eV.[59] The latter two quantities agree with recent high-level ab initio CCSD calculations, which give 3.30 and 7.341 eV, respectively.[60] Given these values, reactions of Mg^+ with CH_3OH to form $MgOH^+ + CH_3$ and $MgOH + CH_3^+$ are endothermic by 0.7 ± 0.2 and 3.2 ± 0.2 eV, respectively. Reaction 5 will be more endothermic by the binding energy of the $Mg^+(CH_3OH)_x$ complex while reaction 4 includes that increase minus the BDEs of $MgOH^+$ to *y* CH_3OH molecules (which are unknown). In

TABLE 4: Optimized Parameters of Eq 1 for CID of $Mg^+(CH_3OH)_x$ and $Mg^+(C_6H_6)$ Complexes with Xe[a]

reactant ion	product ion	σ_0	n	E_0, eV
$Mg^+(CH_3OH)$	Mg^+	8 (1)	1.2 (0.1)	1.51 (0.07)
	$MgXe^+$	1.8 (1.4)	1.6 (0.2)	1.3 (0.1)
	$MgOH^+$	0.10 (0.03)	2.0 (0.1)	5.5 (0.5)
	CH_3^+	0.01 (0.005)	2.6 (0.4)	9.7 (0.5)
$Mg^+(CH_3OH)_2$	$Mg^+(CH_3OH)$	38 (2)	1.0 (0.2)	1.25 (0.07)[b]
	Mg^+	4.4 (1.8)	1.6 (0.3)	2.8 (0.1)
	$Mg^+(CH_3OH)Xe$	0.06 (0.08)	1.5 (0.4)	1.0 (0.1)
	$MgXe^+$	0.32 (0.35)	1.3 (0.3)	2.7 (0.1)
	$MgOH^+(CH_3OH)$	0.04 (0.02)	2.3 (0.2)	7.6 (1.1)
	$MgOH^+$	0.13 (0.09)	2.0 (0.3)	7.0 (1.2)
	CH_3^+	0.14 (0.07)	1.7 (0.2)	16.6 (0.9)
$Mg^+(CH_3OH)_3$	$Mg^+(CH_3OH)_2$	87 (3)	0.8 (0.2)	0.95 (0.09)[c]
	$Mg^+(CH_3OH)$	13 (2)	0.8 (0.3)	2.5 (0.1)
	$MgOH^+(CH_3OH)_2$	0.03 (0.02)	2.2 (0.2)	8.4 (1.2)
$Mg^+(C_6H_6)$	Mg^+	20 (1)	1.3 (0.1)	1.39 (0.10)

[a] Uncertainties in parentheses. [b] Lifetime shift = 0.03 eV. [c] Lifetime shift = 0.06 eV.

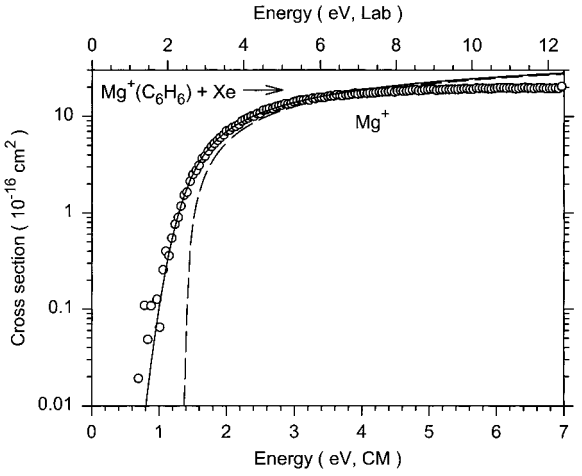

Figure 6. Cross sections for collision-induced dissociation of the $Mg^+(C_6H_6)$ complex with Xe as a function of kinetic energy in the center-of-mass frame (lower *x*-axis) and the laboratory frame (upper *x*-axis). The solid line shows the best fit to the CID cross section using the model of eq 1 convoluted over the neutral and ion kinetic and internal energy distributions. The dotted line shows the model cross section in the absence of experimental kinetic energy broadening for reactants with an internal energy of 0 K.

all cases, the apparent thresholds of reactions 4 and 5 are well above the thermodynamic thresholds. This is partly because of the severe competition with the much more favorable reaction 2, but there may also be barriers to these bond activation processes. Analysis of these cross sections is included in Table 4 for completeness, but the E_0 values have no thermodynamic meaning.

CID of $Mg^+(C_6H_6)$. Cross section results for the interaction of $Mg^+(C_6H_6)$ with Xe are shown in Figure 6. Simple CID to form Mg^+ is the only process observed. It has an apparent threshold near 0.9 eV and a relatively large cross section of about 20×10^{-16} cm^2 at elevated energies. Results of the analysis of this cross section using eq 1 are given in Table 4 and shown in Figure 6.

Theoretical Results

Geometries. Structures for the various magnesium ion clusters studied experimentally and for the bare ligands were calculated as described above. Table 5 gives details of the final geometries for each of these species. In cases where previous calculations have been performed, our results are consistent and differ only slightly due to variations in the levels of theory used,

TABLE 5: MP2(full)/6-31G* Geometry Optimized Structures of $Mg^+(L)_x$ ($x = 1-3$) Complexes[a]

$Mg^+(L)_x$	sym	Mg^+-X distances (Å)	$\angle Mg^+-X-Y$ (deg)	$\angle X-Mg^+-X$ (deg)
$Mg^+(Ar)$	$C_{\infty v}$	2.919 (1)		
$Mg^+(CO)$	$C_{\infty v}$	2.509 (1)	180.0 (1)	
$Mg^+(CO_2)$	$C_{\infty v}$	2.132 (1)	180.0 (1)	
$Mg^+(H_2O)$	C_{2v}	2.065 (1)	126.8 (2)	
$Mg^+(NH_3)$	C_{3v}	2.188 (1)	113.2 (3)	
$Mg^+(CH_4)$	C_{3v}	2.545 (1)	180.0 (1)	
			74.1 (3)	
$Mg^+(CH_3OH)$	C_s	2.037 (1)	129.3 (1)	
$Mg^+(C_6H_6)$	C_{6v}	2.634 (6)	74.5 (2)	
$Mg^+(CO)_2$	C_{2v}	2.479 (2)	173.4 (2)	84.3 (1)
$Mg^+(CO_2)_2$	C_{2v}	2.168 (2)	159.5 (2)	85.9 (1)
$Mg^+(H_2O)_2$	C_2	2.087 (2)	122.7 (2)	91.1 (1)
			127.1 (2)	
$Mg^+(NH_3)_2$	C_{2v}	2.207 (2)	109.0 (2)	101.1 (1)
			115.4 (4)	
$Mg^+(CH_4)_2$	C_{2v}	2.658 (2)	168.1 (2)	95.6 (1)
$Mg^+(CH_3OH)_2$	C_2	2.069 (2)	126.6 (2)	91.8 (1)
$Mg^+(CO)_3$	C_{3v}	2.408 (3)	171.0 (3)	86.9 (3)
$Mg^+(CO_2)_3$	C_{3v}	2.190 (3)	154.7 (3)	85.6 (3)
$Mg^+(H_2O)_3$	C_3	2.112 (3)	120.6 (3)	89.2 (3)
			121.2 (3)	
$Mg^+(NH_3)_3$	C_{3v}	2.219 (3)	109.6 (6)	99.4 (3)
			120.2 (3)	
$Mg^+(CH_3OH)_3$	C_3	2.105 (3)	128.2 (3)	89.9 (3)

[a] X is the atom in the ligand closest to the magnesium cation; Y is the heaviest atom bonded to X. Numbers in parentheses refer to the number of X atoms at this bond distance or the number of angles.

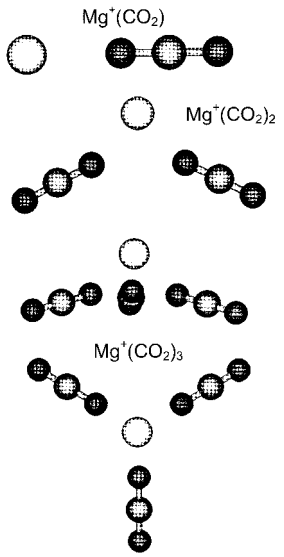

Figure 7. Ground state geometries of $Mg^+(CO_2)_x$ ($x = 1-3$) complexes optimized at the MP2(full)/6-31G* level of theory. Views from the side and above are shown for $x = 3$.

except as noted. Illustrative results for the most stable conformations of several magnesium ion−ligand complexes are shown in Figures 7 and 8. As theoretical results for many of these complexes have been discussed previously in detail,[10,12,15−25] we will only briefly review the qualitative aspects of these results.

The monoligated complexes have geometries that can be anticipated by simple electrostatic considerations. In all cases, the most symmetric complexes possible are formed. When available, lone pairs of electrons on the ligand point at the cation. Species having dipole moments (H_2O, NH_3, and CH_3OH) align the metal ion with the dipole. The linear $Mg^+(CO_2)$ geometry is dictated by interaction of the metal ion with the quadrupole moment of the ligand.[21] The geometry of the $Mg^+(CH_4)$

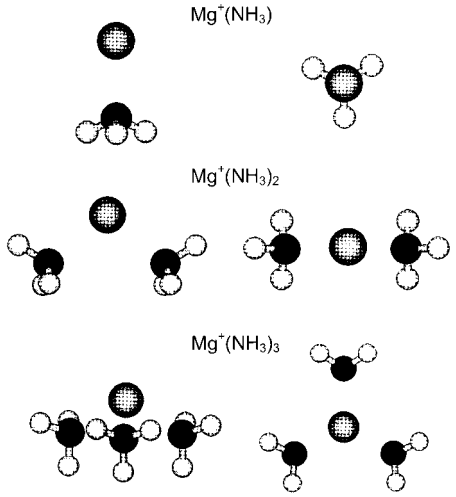

Figure 8. Ground state geometries of $Mg^+(NH_3)_x$ ($x = 1-3$) complexes, optimized at the MP2(full)/6-31G* level of theory, shown from the side and above.

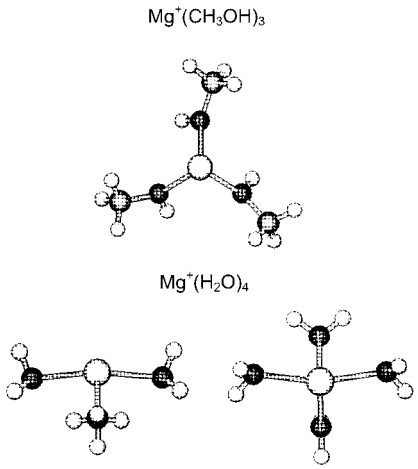

Figure 9. Ground state geometries of $Mg^+(CH_3OH)_3$ and $Mg^+(H_2O)_4$ complexes, optimized at the MP2(full)/6-31G* level of theory. Views from the side and above are shown for the latter complex.

complex is less intuitive. Here, the Mg^+ binds on a 3-fold face of the methane molecule in the so-called η^3 coordination mode, which has C_{3v} symmetry. We verified that the η^2 (C_{2v}) and η^1 (C_{3v}, where a C−H bond points at Mg^+) coordination complexes were stationary points with one and two imaginary frequencies, as previously determined by Bauschlicher and Sodupe.[24] They found relative energies of these three complexes as 0.0, 0.06, and 0.19 eV for η^3, η^2, and η^1, respectively.

As a second ligand is added to the complexes, theoretical calculations show that the geometries are not determined simply by minimizing ligand−ligand repulsion (which would yield linear L−Mg^+−L complexes). Rather, the complexes are all bent with bond angles of 84°−101° for L = CO, CO_2, H_2O, NH_3, CH_4, and CH_3OH, Table 5.[10,12,18,19,21,25] This geometry reduces repulsion between the ligands and the 3s valence electron on Mg^+ which has hybridized away from the ligands by introducing 3p character. This hybridization is favorable for bonding as it partially deshields the Mg^+ nucleus such that the ligands see a higher nuclear charge. In addition, it can be seen that the ligands no longer point directly at the metal ion, i.e., the Mg^+−X−Y bond angles are no longer 180° for L = CO, CO_2, and CH_4. This is less obvious for the H_2O and NH_3 ligands but the Mg^+−X−Y bond angles indicate the same tilting is occurring. We believe that this tilting is a consequence of electron donation into the empty 3s−3p hybrid orbital localized to one side of the metal ion. Except in the case of L = CO, the Mg^+−L bond lengths increase upon addition of the second ligand, as expected for electrostatically bound complexes. The bond shortening in the case of CO is an interesting observation that deserves further theoretical investigation. It should be noted that in their UHF/6-31G* calculations, Lu and Yang found two geometries (having C_1 and C_2 symmetries) for the $Mg^+(CH_3OH)_2$ complex differing only by 0.21 kJ/mol.[12] We find the same two geometries but our calculations indicate that the more symmetric complex is the ground state by 0.25 kJ/mol.

A third ligand adds to the same side of the complex as the first two ligands, again avoiding the polarized valence electron.[12,19,25] Ligand−metal−ligand bond angles in $Mg^+(L)_3$ decrease slightly compared to the $Mg^+(L)_2$ complexes and metal−ligand bond distances increase slightly, except in the case of L = CO where the reverse trend is again observed. Again the ligands do not point directly at the Mg ion, but tilt at Mg^+−X−Y bond angles that are similar to those observed for the $Mg^+(L)_2$ complexes. In the case of $Mg^+(CH_3OH)_3$, Lu and Yang determined a ground state having C_{3v} symmetry (where the methyl groups all point in the same direction away from the metal ion),[12] while our ground state geometry has only C_3 symmetry (where the methyl groups point away from the metal ion but in three different directions to the side). This is shown in Figure 9. Our calculations indicate that the C_{3v} structure collapses to the C_3 structure and lies 9.5 kJ/mol higher in energy at the MP2(full)/6-311+G(2d,2p)//MP2(full)/6-31G* level (no BSSE or ZPE corrections). Structures in which the third water or methanol ligand is bound in a second solvent shell by two hydrogen bonds to the first two ligands have also been considered.[12,25] For the $Mg^+(H_2O)_3$ system, Watanabe et al. (WIHMF) found that this structure lay 17.4 kJ/mol above the ground state structure (MP4SDTQ/6-31G*//SCF/6-31G*), while we find a difference of 8.1 kJ/mol (MP2(full)/6-311+G(2d,2p)//MP2(full)/6-31G* calculations with no BSSE or ZPE corrections). For the methanol system, Lu and Yang found that this structure lay 6.9 kJ/mol above their C_{3v} structure at the SCF/6-31G* level.

In the water and ammonia systems, calculations were also performed for the four ligand complexes. Our results for $Mg^+(NH_3)_4$ are specified in Table 6 and shown in Figure 10. They directly parallel the qualitative geometries observed for $Mg^+(H_2O)_4$ complexes, which have been previously characterized by Bauschlicher and Partridge (BP) at the SCF/6-31G* level[18] and WIHMF at the SCF/6-31G level.[25] BP and WIHMF found that the fourth ligand can bond directly to the metal or in a second solvent shell. Our calculations for $Mg^+(H_2O)_4$ and $Mg^+(H_2O)_3(H_2O)$ are similar to those of these previous studies, although the symmetry of our $Mg^+(H_2O)_4$ complex (obtained using the tight convergence criterion at the MP2(full)/6-31G* level in Gaussian 98) differs slightly in the orientation of the hydrogens. This is shown in Figure 9. We find that this complex has C_s symmetry compared to a C_2 complex found by BP and C_{2v} by WIHMF. We find that the C_{2v} symmetry complex lies only 0.041 eV above the C_s ground state. The latter shows evidence of hydrogen bonding as the complex is distorted from C_{2v} by moving two opposite water molecules closer to the water on one side of the complex (O···H bond distance = 2.632 Å). In agreement with BP and WIHMF, we find that the $Mg^+(H_2O)_3(H_2O)$ is more strongly bound. Our calculations indicate that this structure is more stable by only 0.074 eV (including ZPE and BSSE corrections, 0.10 eV without), while at lower levels of theory, BP find a difference of 0.16 eV (without ZPE or BSSE corrections) and WIHMF find a 0.25 eV difference.

TABLE 6: MP2(full)/6-31G* Geometry Optimized Structures of $Mg^+(L)_x$ ($x = 4-5$) Complexes[a]

$Mg^+(L)_x$	sym	Mg^+-X distances (Å)	$\angle X-Mg^+-X$ (deg)[b]
$Mg^+(H_2O)_4$	C_s	2.111 (2), 2.175 (2)	**81.1** (1), 88.2 (2), 91.7 (2), **161.8** (1)
$Mg^+(H_2O)_3(H_2O)$	C_s	2.090 (1), 2.093 (2), 3.883 (1)	44.3 (2), **85.5** (1), 97.0 (2), **112.5** (1)
$Mg^+(NH_3)_4$	C_{2v}	2.234 (2), 2.275 (2)	90.7 (4), **100.8** (1), **177.7** (1)
$Mg^+(NH_3)_3(NH_3)$	C_s	2.218 (1), 2.204 (2), 4.260 (1)	48.5 (2), **90.8** (1), 101.6 (2), **126.1** (1)
$Mg^+(NH_3)_5$	C_1	2.261 (1), 2.270 (2), 2.273 (2)	88.1 (1), 89.4(2), 89.5 (2), 91.0 (2), 93.2 (1), **177.4** (2)
$Mg^+(NH_3)_4(NH_3)$	C_s	2.216 (2), 2.274 (2), 4.414 (1)	45.9 (2), 91.3 (2), 91.6 (2), **91.8** (1), **175.9** (1)

[a] X is the atom in the ligand closest to the magnesium cation; *Y* is the heaviest atom bonded to X. Numbers in parentheses refer to the number of X atoms at this bond distance or the number of angles. [b] Bolded values refer to ligands opposite (rather than adjacent) to one another.

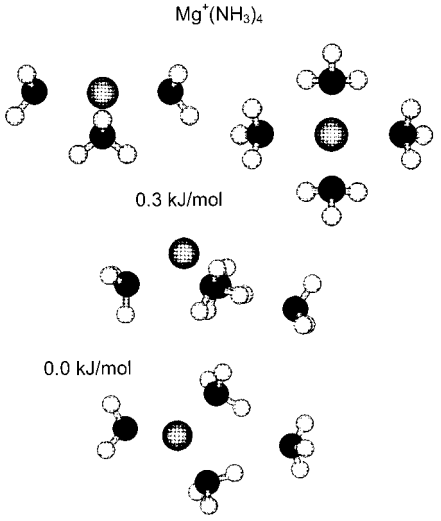

Figure 10. Ground state geometries of the two low-lying forms of the $Mg^+(NH_3)_4$ complexes, optimized at the MP2(full)/6-31G* level of theory, shown from the side and above.

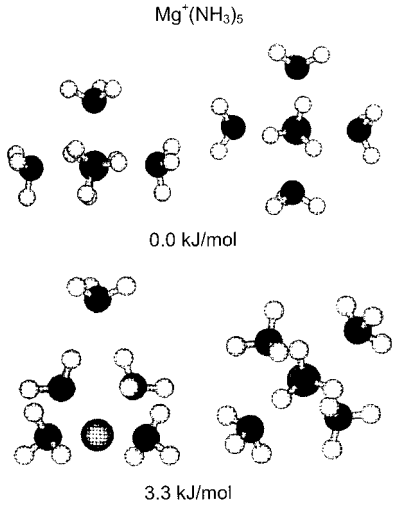

Figure 11. Ground state geometries of the two low-lying forms of the $Mg^+(NH_3)_5$ complexes, optimized at the MP2(full)/6-31G* level of theory, shown from the side and above.

On the basis of the present calculations, the true ground state geometry cannot be determined unambiguously. Similarly, we find that the $Mg^+(NH_3)_4$ and $Mg^+(NH_3)_3(NH_3)$ geometries are very close in energy at the level of theory used here, with the latter more stable by only 0.003 eV (including ZPE and BSSE corrections; 0.075 eV less stable without these corrections). The smaller difference in the relative stability of the two geometries in the ammonia system can be understood qualitatively by noting that in both the water and ammonia complexes, the ligand in the second shell makes two hydrogen bonds with ligands in the first solvent shell, Figure 10. As there are two lone pairs on the oxygen, the two hydrogen bonds are stronger than those formed by the single lone pair on nitrogen.

Finally, we calculated the structure of the $Mg^+(NH_3)_5$ and $Mg^+(NH_3)_4(NH_3)$ complexes, obtaining the results shown in Figure 11. The ground state structure is found to have all five ammonias attached directly to the magnesium ion. These ligands are arrayed approximately 90° away from one another in a roughly square pyramidal orientation. The $Mg^+(NH_3)_4(NH_3)$ geometry is formed by adding the fifth ammonia to the $Mg^+(NH_3)_4$ complex along the C_2 symmetry axis and again forming two hydrogen bonds. This geometry is calculated to lie slightly higher in energy by 0.075 (0.080 eV before ZPE and BSSE corrections).

A crude picture of the bonding in these complexes notes a direct analogy with the valence shell electron pair repulsion (VSEPR) model of freshman chemistry.[61] In this picture, the ligands and the single valence electron are occupying roughly equivalent sites around a dipositive magnesium ion. The system can then distort in response to ligand−electron repulsion and ligand−ligand repulsion, where the former appears to be larger. Thus, the (e)$Mg^+(L)$ complexes are linear, (e)$Mg^+(L)_2$ are trigonal planar, (e)$Mg^+(L)_3$ are tetrahedral, (e)$Mg^+(L)_4$ are trigonal bipyramidal, and (e)$Mg^+(L)_5$ are octahedral.

Bond Energies. Magnesium ion binding energies were determined using the MP2(full)/6-31G* geometries and single point energy calculations performed at the MP2(full)/6-311+G-(2d,2p) level. Values corrected for zero-point energies and BSSE are listed in Table 7 for the ground state. Comparison of these values with those calculated by Bauschlicher and co-workers[15−24] shows fairly good agreement. The largest difference is 0.15 eV for $Mg^+(CO_2)$ and the mean average deviation (MAD) between our values and the 17 SCF and 7 MCPF values is 0.08 ± 0.04 eV. Except for $Mg^+(CO)$ and $Mg^+(C_6H_6)$, our values are systematically lower than those from the literature, which may be a result of including BSSE corrections in the present analysis. Overall the comparison of our theoretical bond energies to those in the literature is quite satisfactory.

Discussion

Thresholds for the primary CID processes, reactions 2, listed in Tables 1−4 are taken to equal the 0 K bond dissociation energies (BDEs). Thresholds for the loss of subsequent ligands from multiligated complexes provide BDEs that are generally higher because of competition with the more favorable primary dissociation channel. Hence, the final thermochemistry listed in Table 7 is taken exclusively from the thresholds for loss of a single ligand. We also found that kinetic shifts are generally small and observed only for more complicated species with larger thresholds,[42] i.e., $Mg^+(CO_2)_3$, $Mg^+(CH_3OH)_x$ ($x = 2, 3$), and $Mg^+(NH_3)_x$ ($x = 4, 5$). These kinetic shifts are specified in Tables 2−4.

We can also obtain information regarding $MgAr^+$ and $MgXe^+$ from the thresholds for formation of these ions in the $Mg^+(CO)$, $Mg^+(CO_2)_{1,2}$, and $Mg^+(CH_4)$ systems compared to the

TABLE 7: Bond Dissociation Energies at 0 K of Mg^+−Ligand Complexes (in eV)

	this work		literature		
bond	CID[a]	theory[b]	theory[c]	PD	FTICR
Mg^+-Ar	0.10 (0.07)	0.07	0.13* [0.12*][d]	0.16[e]	
Mg^+-Xe	0.32 (0.12)			0.52[e]	
Mg^+-CO	0.43 (0.06)	0.44	0.31 [0.39][f]		
$(CO)Mg^+-CO$	0.40 (0.03)	0.40			
$(CO)_2Mg^+-CO$		0.44			
Mg^+-CO_2	0.60 (0.06)	0.56	0.63 [0.71][g]	0.64[h]	
$(CO_2)Mg^+-CO_2$	0.50 (0.03)	0.42	0.44* [0.46*][g]		
$(CO_2)_2Mg^+-CO_2$	0.46 (0.06)	0.34			
Mg^+-OH_2	1.23 (0.13)[i]	1.23	1.32[j,k] [1.33][l]	1.05[m]	2.60 (0.22)[n]
$(H_2O)Mg^+-OH_2$	0.97 (0.07)[i]	0.98	1.05[j−l]		
$(H_2O)_2Mg^+-OH_2$	0.75 (0.09)[i]	0.80	0.84*[j,k]		
$(H_2O)_3Mg^+-OH_2$	0.50 (0.09)[i]	0.51 {0.58}	0.39* {0.58*}[j,k]		
Mg^+-NH_3	1.60 (0.12)	1.54	1.60*[j] [1.63][f]		
$(NH_3)Mg^+-NH_3$	1.27 (0.07)	1.15	1.20*[j]		
$(NH_3)_2Mg^+-NH_3$	0.99 (0.09)	0.92	0.94*[j]		
$(NH_3)_3Mg^+-NH_3$	0.45 (0.11)	0.48 {0.49}			
$(NH_3)_4Mg^+-NH_3$	0.58 (0.12)	0.44 {0.37}			
Mg^+-CH_4	0.29 (0.07)	0.28	0.17 [0.33][o]		
$(CH_4)Mg^+-CH_4$	0.15 (0.07)	0.17			
Mg^+-CH_3OH	1.51 (0.07)	1.47	1.49 [1.56][l]		2.65 (0.22)[p]
$(CH_3OH)Mg^+$- CH_3OH	1.25 (0.07)	1.13	1.25[k]		
$(CH_3OH)_2Mg^+$- CH_3OH	0.95 (0.09)	0.90			
$Mg^+-C_6H_6$	1.39 (0.10)	1.37	1.32[f]	≤1.17[q]	

[a] Uncertainties in parentheses. Values taken from Tables 1−4. [b] MP2(full)/6-311+G (2d,2p)//MP2 (full)/6-31G* calculations. Values in braces are for species where the outermost ligand is in the second solvent shell. [c] SCF [MCPF] values. Stars indicate values corrected for zero-point energies using vibrational frequencies calculated here. [d] Reference 14. [e] Reference 3. [f] Reference 10. [g] Reference 15. [h] Reference 5 [i] Reference 8. [j] Reference 13. [k] Reference 12. [l] Reference 11. [m] Reference 4. [n] Reference 2. [o] Reference 18. [p] Reference 1. [q] Reference 6.

thresholds for formation of Mg^+. Our best value for $D(Mg^+-Ar)$, Table 7, is the average of the values obtained from the $Mg^+(CO)$ and $Mg^+(CH_4)$ systems, 0.12 ± 0.12 and 0.07 ± 0.08 eV, respectively. Our best value for $D(Mg^+-Xe)$, Table 7, is the average of the two values obtained in the $Mg^+(CO_2)_{1,2}$ systems, 0.30 ± 0.11 and 0.35 ± 0.16 eV, respectively. Note that these values agree with our observations that the ligand exchange reaction 3 of $Mg^+(CH_4)$ with Xe is exothermic, while that with Ar is endothermic. Thus, $D(Mg^+-CH_4)$ lies between the magnesium ion BDEs to the two rare gas atoms. For completeness, Table 7 also provides the BDEs for the $Mg^+(H_2O)_x$ ($x = 1-4$) complexes that were previously determined in our laboratory.[7]

Comparison of Theoretical and Experimental Bond Energies. Table 7 compares our experimental BDEs with those calculated by Bauschlicher et al.[15−24] This comparison is very gratifying. For the 15 complexes where there is both a CID and theory value, the MAD between the SCF theoretical values and our experimental values is 0.06 ± 0.04 eV. The seven values calculated at the higher MCPF level of theory exhibit the same good agreement with our experimental values (MAD of 0.06 $\pm$ 0.04 eV). In almost all cases, the differences between experiment and theory are within experimental error.

Comparably good agreement is obtained for all complexes when the present calculations are compared to our experimental values. For 21 complexes, the MAD is 0.05 ± 0.04 eV. The largest deviation is 0.14 eV for the $Mg^+(NH_3)_5$ complex. The agreement is shown in Figure 12, which also shows that the trends in theory and experiment are match well. Theoretical values for the CO_2, NH_3, and CH_3OH complexes appear to be systematically low, while those for the other complexes agree very well with experiment.

Comparison with Experimental Bond Energies from the Literature. Table 7 also includes the experimental values from the photodissociation (PD) work of Operti et al.[1,2] and Duncan and co-workers.[3−6] The agreement with this work is clearly less satisfactory. For the rare gas complexes, our experimental values

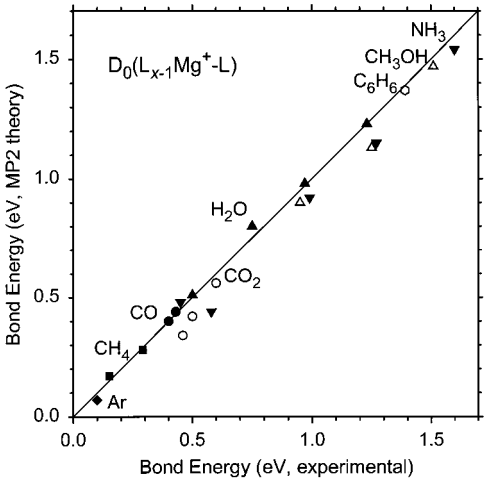

Figure 12. Theoretical vs experimental bond dissociation energies (in eV) for $(L_{x-1})Mg^+-L$. All values are at 0 K and are taken from Table 7. Theory is represented by the present calculations at the MP2(full)/6-311+G(2d,2p)//MP2(full)/6-31G* level. The diagonal line indicates the values for which calculated and measured bond dissociation energies are equal.

are not very precise, but the value for $MgAr^+$ does agree with theory[20] and is within experimental error of the PD value. For $MgXe^+$, our value lies considerably below the PD value and there is no theory for comparison. This discrepancy may be because of the limitations associated with the Birge−Sponer extrapolation used to obtain the PD values. This is because an electrostatically bound complex may not be well described by a Morse potential.[3,4] In this case, this may be because the excited potential surface accessed in the PD experiments is almost degenerate with the potential energy surface corresponding to the $Mg + Xe^+$ charge transfer asymptote.[62] The error could also be with our values, which are derived from the relative thresholds of reactions 2 and 3, making them less precise than all other values obtained here. We believe the agreement in these

TABLE 8: Enthalpies and Free Energies for $L_{x-1}Mg^+-L$ at 0 and 298 K in kJ/mol[a]

system	ΔH_0[b]	$\Delta H_{298} - \Delta H_0$[c]	ΔH_{298}	$T\Delta S_{298}$[c]	ΔG_{298}
$Mg^+(Ar)$	9.6 (6.8)	1.7 (0.2)	11.3 (6.8)	17.2 (0.2)	−5.9 (6.8)
$Mg^+(CO)$	41.5 (5.8)	1.6 (0.3)	43.1 (5.8)	26.8 (0.7)	16.3 (5.8)
$Mg^+(CO)_2$	38.6 (2.9)	0.7 (0.3)	39.4 (2.9)	31.4 (1.0)	8.0 (2.9)
$Mg^+(CO_2)$	57.9 (5.8)	0.5 (0.2)	58.4 (5.8)	30.8 (0.8)	27.6 (5.8)
$Mg^+(CO_2)_2$	48.2 (2.9)	−0.4 (0.3)	47.8 (2.9)	20.8 (1.5)	27.0 (2.9)
$Mg^+(CO_2)_3$	44.4 (5.8)	−1.4 (0.2)	43.0 (5.8)	32.5 (1.3)	10.5 (5.8)
$Mg^+(H_2O)$	118.7 (12.5)	3.8 (0.3)	122.5 (12.5)	28.1 (0.6)	94.4 (12.5)
$Mg^+(H_2O)_2$	93.6 (6.8)	2.1 (0.5)	95.7 (6.8)	33.4 (1.3)	62.3 (6.8)
$Mg^+(H_2O)_3$	72.4 (8.7)	3.1 (0.6)	75.5 (8.7)	42.2 (1.3)	33.3 (8.7)
$Mg^+(H_2O)_4$	48.2 (8.7)	1.6 (0.5)	49.8 (8.7)	35.9 (1.4)	13.9 (8.7)
$Mg^+(NH_3)$	154.4 (11.6)	4.5 (0.3)	158.9 (11.6)	30.1 (0.5)	128.8 (11.6)
$Mg^+(NH_3)_2$	122.5 (6.8)	1.4 (0.5)	123.9 (6.8)	29.0 (1.5)	94.9 (6.8)
$Mg^+(NH_3)_3$	95.5 (8.7)	2.3 (0.5)	97.8 (8.7)	42.6 (1.3)	55.2 (8.7)
$Mg^+(NH_3)_4$	44.4 (10.6)	1.0 (0.4)	45.4 (10.6)	33.3 (1.4)	12.2 (10.6)
$Mg^+(NH_3)_5$	56.0 (11.6)	1.0 (0.4)	57.0 (11.6)	38.9 (1.3)	18.1 (11.6)
$Mg^+(CH_4)$	28.0 (6.8)	1.8 (0.3)	29.8 (6.8)	21.8 (0.7)	8.0 (6.8)
$Mg^+(CH_4)_2$	14.5 (6.8)	−1.7 (0.3)	12.8 (6.8)	19.8 (1.5)	−7.0 (6.8)
$Mg^+(CH_3OH)$	145.7 (6.8)	1.9 (0.2)	147.6 (6.8)	28.2 (0.7)	119.4 (6.8)
$Mg^+(CH_3OH)_2$	121.6 (6.8)	−0.4 (0.4)	121.2 (6.8)	39.9 (1.5)	81.3 (6.8)
$Mg^+(CH_3OH)_3$	92.6 (8.7)	−0.3 (0.4)	92.3 (8.7)	43.0 (1.5)	49.3 (8.7)
$Mg^+(C_6H_6)$	134.1 (9.6)	1.9 (0.2)	136.0 (9.6)	31.2 (0.6)	104.8 (9.6)

[a] Uncertainties are listed in parentheses. [b] Experimental values from this work, Table 7. [c] Calculated using standard formulas and molecular constants calculated at the MP2(full)/6-31G* level. For experimentally studied complexes, the molecular constants are given in Tables S1 and S2. Uncertainties correspond to 10% variations in the vibrational frequencies.

two cases is satisfactory given the interpretational difficulties in both experiments.

For the case of $Mg^+(CO_2)$, both experimental values and theory are in excellent agreement with each other and with theory. For the case of $Mg^+(C_6H_6)$, our value is slightly greater than both theoretical values, but well within experimental uncertainty. The value obtained by Willey et al.[6] (technically an upper limit) is somewhat below the other values. A similar discrepancy between our CID results[63] and PD results of Duncan et al.[6,64,65] has also been obtained for the analogous complex, $Ag^+(C_6H_6)$. Here too, our CID value of 1.62 ± 0.07 eV agrees better with theory (1.58 ± 0.22 eV)[66] than the PD value (1.31 eV). One plausible interpretation for the lower value in the PD data is that there is residual internal energy in the complex that is not accounted for in the PD threshold measurement. It is presumed that the supersonic jet expansion used to produce these complexes yields a cold distribution of internal energies, but not all degrees of freedom may cool efficiently.

The case of $Mg^+(H_2O)$ has been discussed previously[7] but here too the PD value from Duncan's laboratory[4] is somewhat below both our CID value and theory.[17−19] Again, this difference could be simply a limitation of the Birge−Sponer extrapolation used in this system to obtain the bond energy, especially as a "pseudo-diatomic" approximation was used.[62] The value from the work of Freiser and co-workers[2] is clearly inaccurate as is that for the $Mg^+(CH_3OH)$ complex.[1] Operti et al. observe photodissociation at about 2.6 eV for $Mg^+(L)$ complexes where L = H_2O, CH_3OH, C_2H_5OH, $(CH_3)_2CHOH$, $(CH_3)_2CO$, and $(CH_3)CO(C_2H_5)$. Apparently, the Mg^+ complexes generated in this work have a strong absorption in this energy region with a band that may shift slightly with differing ligands. It is not clear what this absorption corresponds to as the lowest excitation in the atomic ion ($^2P \leftarrow {}^2S$) lies at 4.43 eV.[67] In the $Mg^+(H_2O)$ complex ($^2A_1$ ground state), Willey et al. find that this atomic transition is red-shifted to 3.52 eV,[4] but this is still well above the energy found by Freiser and co-workers. The dichotomy of assigning the absorption at 2.6 eV has also been discussed for the $Mg^+(CH_3OH)$ system by Bauschlicher and Partridge.[17] They calculate a red-shifted atomic absorption at 3.44 eV with no other low-lying states present. We agree with their speculation that the complexes in the study of Operti et al. probably had appreciable internal energies allowing the atomic $^2P \leftarrow {}^2S$ transition to be accessed at about 2.6 eV. Once excited, the complexes may either predissociate or absorb a second photon.

Conversion from 0 to 298 K. To allow comparison to commonly used experimental conditions, we convert the 0 K bond energies determined here to 298 K bond enthalpies and free energies. The enthalpy conversions are calculated using rigid rotor/harmonic oscillator approximations and the vibrational and rotational constants determined using MP2(full)/6-31G* calculations, such as those given in Tables S1 and S2. Table 8 lists 0 and 298 K enthalpy, free energy, and enthalpic and entropic corrections for all systems experimentally determined. Uncertainties in these values are determined by 10% variations in the molecular constants. While this undoubtedly overestimates the errors associated with higher vibrational frequencies, it may underestimate errors for the low frequencies that turn into rotations and translations upon dissociation. It should be noted that in previous work we have found that it is inappropriate to treat such vibrations as internal rotors in the interpretation of the data.[68] Overall, the enthalpy and entropy corrections and derived ΔG_{298} values listed in Table 8 should be viewed as first approximations.

Among the experimental information available in the literature are relative free energies at 298 K, ΔG_{298}(rel), measured by Operti et al.[1] using equilibrium methods. These were placed on an absolute scale by referencing to an absolute bond energy for $Mg^+(CH_3OH)$ determined by photodissociation. Having reassigned this latter value, the relative values for 11 species can now be placed on an absolute scale for use in other experiments. Using the information in Table 8, the relative values can be adjusted to absolute free energies at 298 K and are listed in Table 9. Unfortunately, the molecular information needed to convert these quantities to bond enthalpies at 0 or 298 K are not available. However, Operti et al. point out that to a reasonable approximation, the enthalpic and entropic corrections for the species in Table 9 are not that different, such that a first approximation to the bond energies are also given in Table 9.

Trends in the Mg^+-Ligand Binding Energies. The bond dissociation energies (BDEs) listed in Table 7 are shown pictorially in Figure 13. Concentrating first on the binding between a single ligand and Mg^+, we find that the ligands clearly

TABLE 9: Reassigned Absolute Bond Energies Determined by Operti et al.[1]

L	ΔG_{298}(rel),[a] kJ/mol	ΔG_{298}(abs),[b] kJ/mol	ΔH_0(abs),[c] eV
CH_3OH	0.0	119.4[d]	1.51[e]
C_2H_5OH	7.4	126.8	1.59
CH_3CHO	9.5	128.9	1.61
n-C_3H_7OH	12.3	131.7	1.64
i-C_3H_7OH	15.0	134.4	1.67
C_2H_5CHO	15.4	134.8	1.67
n-C_4H_9OH	16.2	135.6	1.68
n-C_3H_7CHO	19.2	138.6	1.71
$(C_2H_5)_2O$	21.6	141.0	1.73
THF[f]	22.6	142.0	1.74
$(CH_3)_2CO$	26.8	146.2	1.79
$(CH_3)CO(C_2H_5)$	32.0	151.4	1.84

[a] Values from ref 1. Uncertainties are ±0.4 kJ/mol. [b] Uncertainties are ±6.8 kJ/mol. [c] Uncertainties are ±0.07 eV. [d] From Table 8. [e] From Table 7. [f] Tetrahydrofuran.

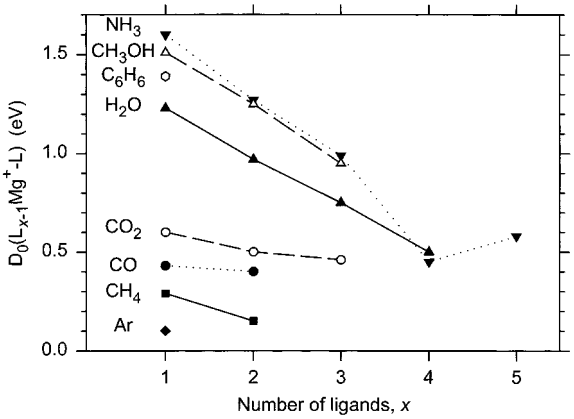

Figure 13. Experimental bond dissociation energies as a function of the number of ligands. Data taken from Table 7.

fall into two major categories. Strongly bound ligands include water, ammonia, methanol, and benzene. Weakly bound ligands include carbon monoxide, carbon dioxide, and methane. (The rare gases would also be included in this category.) As all these ligands are closed-shell species, it is reasonable to assume that the bonding between Mg^+ and these neutral ligands is governed primarily by ion−dipole, ion−quadrupole, and ion−induced dipole interactions. Water, ammonia, and methanol have sizable dipole moments while none of the other ligands do, helping to explain why they have strong BDEs with Mg^+. Benzene has the largest polarizability among all the ligands and can be thought of as a six-electron donor, while all other ligands are essentially two-electron donors. This explains why the benzene BDE is also among the highest measured.

Experimentally, we find that the second ligand is weaker than the first by almost the same factor in all complexes but L = CO and CH_4. The average ratio of the second to first ligand BDE is 0.81 ± 0.13 for L = CO_2, H_2O, NH_3, and CH_3OH. The theoretical calculations for these four complexes find a ratio of 0.77 ± 0.03, in good agreement with the experimental result. For L = CO, theory and experiment agree that the second BDE is about 92% of the first. We believe this is probably because there is much less ligand−ligand repulsion in this case. We note that the L−Mg^+−L bond angle (84.3°) is the smallest for the $Mg^+(CO)_2$ complex. Likewise, calculations by Bauschlicher and Partridge[15] on $MgAr_x^+$ complexes (x = 1 and 2) show that the first and second Mg^+−Ar BDEs are essentially identical and that the Ar−Mg^+−Ar bond angle is 82.5°. The reduced ligand−ligand repulsion in the Ar and CO systems allows the ligands to avoid the hybridized 3s electron more effectively (which should also enhance the hybridization). In contrast to these small ligands, we find that the second methane bond energy is about half of the first methane BDE (60% theoretically). Similarly, Bauschlicher and Partridge have calculated that the BDE of a second benzene molecule to Mg^+ is less than half that of the first benzene.[18] In the latter case, the angle between the center of the benzene rings and Mg^+ is 148°. Because this ligand is so much larger than the others considered here, there is clearly much more ligand−ligand repulsion.

When a third ligand is added to the magnesium ion, we find a similar consistency for the average ratio of the third to first ligand BDE determined experimentally, namely 0.62 ± 0.12 for L = H_2O, NH_3, and CH_3OH. (Note that this means the ratio for the third to second ligands is 0.77 ± 0.12, the same value as the first to second metal−ligand bond energy ratio.) Our theoretical calculations find a ratio of 0.61 ± 0.03, again in good agreement with the experimental results. Theoretically, a similar ratio is obtained for the CO_2 ligand sequence; however, experimentally the third CO_2 is 77 ± 18% of the first. This could indicate that our $(CO_2)Mg^+$−CO_2 BDE should lie toward the lower end of the experimental limits.

As noted above, in the water and ammonia systems, there are two possible geometries for addition of a fourth and fifth ligand. The trend in the experimental $(H_2O)Mg^+$−OH_2 BDEs (Figure 13) shows no obvious break between the third and fourth ligand. Such a break has been taken as an indication of a change in solvent shell. Theory, however, suggests that the fourth water molecule binds more tightly in the second solvent shell because of the strong hydrogen bonding. In contrast, the fourth and fifth ammonia ligands are much more weakly bound than the first three ligands, a trend that seems consistent with the idea that the fourth and fifth ammonia ligands bind in the second solvent shell through hydrogen bonds. Again calculations indicate that while there is a stable geometry for the fourth and fifth ammonia ligands in the second solvent shell, the most stable geometries have all five ammonias attached directly to Mg^+. The calculated bond energies are in reasonable agreement with experiment (Table 7). Thus, we conclude that ligand−ligand repulsion and steric congestion is responsible for the decline in the bond energies. Further, these examples make it clear that the use of "breaks" in the sequence of metal−ligand bond energies is an unreliable means of determining the extent of solvent shells.

Conclusion

Bond dissociation energies of MgL_x^+ for L = CO (x = 1−2), CO_2 (x = 1−3), NH_3 (x = 1−5), CH_4 (x = 1−2), CH_3OH (x = 1−3), and C_6H_6 (x = 1) are determined by threshold collision-induced dissociation. The experimental values are summarized in Table 7. They are in good agreement with theory values determined by Bauschlicher and co-workers[16−24] for many of the complexes and with MP2(full)/6-311+G(2d,2p)//MP2(full)/6-31G* calculations for all complexes studied. Our experimental values agree reasonably well with photodissociation results of Duncan and co-workers[3,5] for the monoligated rare gas and carbon dioxide complexes, but photodissociation results obtained by Duncan and co-workers[4,6] for water and benzene complexes are low compared to theory and our experiments. Photodissociation results from Freiser and co-workers[1,2] are clearly incorrect and much higher than our experimental values and theory. Geometries of these complexes are determined by the strong interactions between the ligands and the valence electron on Mg^+, which is strongly polarized away from the ligands. Extensive hydrogen bonding in the cases of water and ammonia

lead to the possibility of multiple structures for the fourth and fifth ligands.

Acknowledgment. This work is supported by the National Science Foundation, Grant CHE-9877162 and by the NSF-REU program.

Supporting Information Available: Tables of vibrational frequencies, rotational constants, and detailed computational results (absolute energies calculated with double and triple-ζ basis sets along with zero-point energies and basis set superposition errors) for all complexes. This material is available free of charge via the Internet at http://pubs.acs.org.

References and Notes

(1) Operti, L.; Tews, E. C.; Freiser, B. S. *J. Am. Chem. Soc.* **1988**, *110*, 3847.

(2) Operti, L.; Tews, E. C.; MacMahon, T. J.; Freiser, B. S. *J. Am. Chem. Soc.* **1989**, *111*, 9152.

(3) Pilgrim, J. S.; Yeh, C. S.; Berry, K. R.; Duncan, M. A. *J. Chem. Phys.* **1994**, *100*, 7945.

(4) Willey, K. F.; Yeh, C. S.; Robbins, D. L.; Pilgrim, J. S.; Duncan, M. A. *J. Chem. Phys.* **1992**, *97*, 8886.

(5) Yeh, C. S.; Willey, K. F.; Robbins, D. L.; Pilgrim, J. S.; Duncan, M. A. *J. Chem. Phys.* **1993**, *98*, 1867.

(6) Willey, K. F.; Yeh, C. S.; Robbins, D. L.; Duncan, M. A. *J. Phys. Chem.* **1992**, *96*, 9106.

(7) Dalleska, N. F.; Tjelta, B. L.; Armentrout, P. B. *J. Phys. Chem.* **1994**, *98*, 4191.

(8) Misaizu, F.; Sanekata, M.; Tsukamoto, K.; Fuke, K.; Iwata, S.; *J. Phys. Chem.* **1992**, *96*, 8259. Fuke, K.; Misaizu, F.; Sanekata, M.; Tsukamoto, K.; Iwata, S.; *Z. Phys.* **1993**, *D26*, S180. Misaizu, F.; Sanekata, M.; Fuke, K.; Iwata, S.; *J. Chem. Phys.* **1994**, *100*, 1161.

(9) Sanekata, M.; Misaizu, F.; Fuke, K.; Iwata, S.; Hashimoto, K. *J. Am. Chem. Soc.* **1995**, *117*, 747.

(10) Harms, A. C.; Khanna, S. N.; Chen, B.; Castleman, A. W., Jr. *J. Chem. Phys.* **1994**, *100*, 3540.

(11) Woodward, C. A.; Dobson, M. P.; Stace, A. J. *J. Phys. Chem.* **1997**, *101*, 2279.

(12) Lu, W.; Yang, S. *J. Phys. Chem. A* **1998**, *102*, 825.

(13) France, M. R.; Pullins, S. H.; Duncan, M. A. *Chem. Phys.* **1998**, *239*, 447.

(14) Cheng, Y. C.; Chen, J.; Ding, L. N.; Wong, T. H.; Kleiber, P. D. *J. Chem. Phys.* **1996**, *104*, 6452.

(15) Bauschlicher, Jr., C. W.; Partridge, H.; Langhoff, S. R. *Chem. Phys. Lett.* **1990**, *165*, 272.

(16) Bauschlicher, Jr., C. W.; Partridge, H. *Chem. Phys. Lett.* **1991**, *181*, 129.

(17) Bauschlicher, Jr., C. W.; Partridge, H. *J. Phys. Chem.* **1991**, *95*, 3946.

(18) Bauschlicher, Jr., C. W.; Partridge, H. *J. Phys. Chem.* **1991**, *95*, 9694.

(19) Bauschlicher, Jr., C. W.; Sodupe, M.; Partridge, H. *J. Chem. Phys.* **1992**, *96*, 4453.

(20) Partridge, H.; Bauschlicher, Jr., C. W.; Langhoff, S. R. *J. Phys. Chem.* **1992**, *96*, 5350.

(21) Sodupe, M.; Bauschlicher, Jr., C. W.; Partridge, H. *Chem. Phys. Lett.* **1992**, *192*, 185.

(22) Sodupe, M.; Bauschlicher, Jr., C. W. *Chem. Phys. Lett.* **1992**, *195*, 494.

(23) Bauschlicher, Jr., C. W. *Chem. Phys. Lett.* **1993**, *201*, 11.

(24) Bauschlicher, Jr., C. W.; Sodupe, M. *Chem. Phys. Lett.* **1993**, *214*, 489.

(25) Watanabe, H.; Iwata, S.; Hashimoto, K.; Misaizu, F.; Fuke, K. *J. Am. Chem. Soc.* **1995**, *117*, 755.

(26) Ervin, K. M.; Armentrout, P. B. *J. Chem. Phys.* **1985**, *83*, 166.

(27) Schultz, R. H.; Armentrout, P. B. *Int. J. Mass Spectrom. Ion Processes* **1991**, *107*, 29.

(28) Schultz, R. H.; Crellin, K. C.; Armentrout, P. B. *J. Am. Chem. Soc.* **1992**, *113*, 8590.

(29) Schultz, R. H.; Armentrout, P. B. *J. Chem. Phys.* **1992**, *96*, 1046.

(30) Khan, F. A.; Clemmer, D. C.; Schultz, R. H.; Armentrout, P. B. *J. Phys. Chem.* **1993**, *97*, 7978.

(31) Fisher, E. R.; Kickel, B. L.; Armentrout, P. B. *J. Phys. Chem.* **1993**, *97*, 10204.

(32) Dalleska, N. F.; Honma, K.; Armentrout, P. B. *J. Am. Chem. Soc.* **1993**, *115*, 12125.

(33) Beyer, T. S.; Swinehart, D. F. *Comm. Assoc. Comput. Machines* **1973**, *16*, 379. Stein, S. E.; Rabinovitch, B. S. *J. Chem. Phys.* **1973**, *58*, 2438; *Chem. Phys. Lett.* **1977**, *49*, 1883. Gilbert, R. G.; Smith, S. C. *Theory of Unimolecular and Recombination Reactions*; Blackwell Scientific Publications: Oxford, UK, 1990.

(34) Rodgers, M. T.; Armentrout, P. B. *J. Phys. Chem. A* **1997**, *101*, 2614.

(35) Rodgers, M. T.; Ervin, K. M.; Armentrout, P. B. *J. Chem. Phys.* **1997**, *106*, 4499.

(36) Waage, E. V.; Rabinovitch, B. S. *Chem. Rev.* **1970**, *70*, 377.

(37) Chesnavich, W. J.; Bowers, M. T. *J. Phys. Chem.* **1979**, *83*, 900.

(38) Armentrout, P. B. In *Advances in Gas Phase Ion Chemistry*; Adams, N. G., Babcock, L. M., Eds.; JAI: Greenwich, CT, 1992; Vol. 1, pp 83−119.

(39) See, for example: Sunderlin, L. S.; Armentrout, P. B. *Int. J. Mass Spectrom. Ion Processes* **1989**, *94*, 149.

(40) Dalleska, N. F.; Honma, K.; Sunderlin, L. S.; Armentrout, P. B. *J. Am. Chem. Soc.* **1994**, *116*, 3519.

(41) More, M. B.; Glendening, E. D.; Ray, D.; Feller, D.; Armentrout, P. B. *J. Phys. Chem.* **1996**, *100*, 1605. Ray, D.; Feller, D.; More, M. B.; Glendening, E. D.; Armentrout, P. B. *J. Phys. Chem.* **1996**, *100*, 16116. More, M. B.; Ray, D.; Armentrout, P. B. *J. Phys. Chem. A* **1997**, *101*, 831.

(42) Rodgers, M. T.; Armentrout, P. B. *J. Phys. Chem. A* **1997**, *101*, 1238.

(43) See for example, Figure 1 in ref 32.

(44) Armentrout, P. B.; Simons, J. *J. Am. Chem. Soc.* **1992**, *114*, 8627.

(45) *Gaussian 98*, Revision A.3; Frisch, M. J.; Trucks, G. W.; Schlegel, H. B.; Scuseria, G. E.; Robb, M. A.; Cheeseman, J. R.; Zakrzewski, V. G.; Montgomery, J. A., Jr.; Stratmann, R. E.; Burant, J. C.; Dapprich, S.; Millam, J. M.; Daniels, A. D.; Kudin, K. N.; Strain, M. C.; Farkas, O.; Tomasi, J.; Barone, V.; Cossi, M.; Cammi, R.; Mennucci, B.; Pomelli, C.; Adamo, C.; Clifford, S.; Ochterski, J.; Petersson, G. A.; Ayala, P. Y.; Cui, Q.; Morokuma, K.; Malick, D. K.; Rabuck, A. D.; Raghavachari, K.; Foresman, J. B.; Cioslowski, J.; Ortiz, J. V.; Stefanov, B. B.; Liu, G.; Liashenko, A.; Piskorz, P.; Komaromi, I.; Gomperts, R.; Martin, R. L.; Fox, D. J.; Keith, T.; Al-Laham, M. A.; Peng, C. Y.; Nanayakkara, A.; Gonzalez, C.; Challacombe, M.; Gill, P. M. W.; Johnson, B.; Chen, W.; Wong, M. W.; Andres, J. L.; Gonzalez, C.; Head-Gordon, M.; Replogle, E. S.; Pople, J. A. Gaussian, Inc.: Pittsburgh, PA, 1998.

(46) Møller, C.; Plesset, M. S. *Phys. Rev.* **1934**, *46*, 618.

(47) Bartlett, R. J. *Annu. Rev. Phys. Chem.* **1981**, *32*, 359.

(48) Hehre, W. J.; Radom, L.; Schleyer, P. v. R.; Pople, J. A. *Ab initio Molecular Orbital Theory*; Wiley: New York, 1986.

(49) Hoyau, S.; Norrman, K.; McMahon, T. B.; Ohanessian, G. *J. Am. Chem. Soc.* **1999**, *121*, 8864.

(50) Armentrout, P. B.; Rodgers, M. T. *J. Phys. Chem. A*, in press.

(51) *Exploring Chemistry with Electronic Structure Methods*, 2nd ed.; Foresman, J. B., Frisch, Æ., Eds.; Gaussian: Pittsburgh, PA, 1996.

(52) Boys, S. F.; Bernardi, R. *Mol. Phys.* **1970**, *19*, 553.

(53) Van Duijneveldt, F. B.; van Duijneveldt-van de Rijdt, J. G. C. M.; van Lenthe, J. H. *Chem. Rev.* **1994**, *94*, 1873.

(54) Hill, S. E.; Glendening, E. D.; Feller, D. *J. Phys. Chem. A* **1997**, *101*, 6125. Hill, S. E.; Feller, D.; Glendening, E. D. *J. Phys. Chem. A* **1998**, *102*, 3813.

(55) Nicholas, J. B.; Hay, B. P.; Dixon, D. A. *J. Phys. Chem.* **1999**, *103*, 1394.

(56) Aristov, N.; Armentrout, P. B. *J. Phys. Chem.* **1986**, *90*, 5135.

(57) Hales, D. A.; Armentrout, P. B. *J. Cluster Science* **1990**, *1*, 127.

(58) Berkowitz, J.; Ellison, G. B.; Gutman, D. *J. Phys. Chem.* **1994**, *98*, 2744.

(59) Murad, E. *J. Chem. Phys.* **1981**, *75*, 4080.

(60) Chen, Q.; Milburn, R. K.; Hopkinson, A. C.; Bohme, D. K.; Goodings, J. M. *Int. J. Mass Spectrom.* **1999**, *184*, 153.

(61) Gillespie, R. J. *J. Chem. Educ.* **1963**, *40*, 295.

(62) Duncan, M. A., personal communication.

(63) Chen, Y.-M.; Armentrout, P. B. *Chem. Phys. Lett.* **1993**, *210* , 123.

(64) Willey, K. F.; Cheng, P. Y.; Pearce, K. D.; Duncan, M. A. *J. Phys. Chem.* **1990**, *94*, 4769.

(65) Willey, K. F.; Cheng, P. Y.; Bishop, M. B.; Duncan, M. A. *J. Am. Chem. Soc.* **1991**, *113*, 4721.

(66) Bauschlicher, Jr., C. W.; Partridge, H.; Langhoff, S. R. *J. Phys. Chem.* **1992**, *96*, 3273.

(67) Moore, C. E. Atomic Energy Levels; NSRDS−NBS, 467; U.S. Government Printing Office, Washington, DC, 1949.

(68) Rodgers, M. T.; Armentrout, P. B. *J. Phys. Chem. A* **1999**, *103*, 4955.